# Concurrent Optical Ultrasound and CT Imaging

Fraser T. Watt*,†, Edward Z. Zhang*,†, Paul C. Beard*,†, Erwin J. Alles*,†,

*Wellcome / EPSRC Centre for Interventional and Surgical Sciences, University College London, London, UK
†Department of Medical Physics & Biomedical Engineering, University College London, London, UK

*Abstract*—Optical ultrasound imaging is an emerging paradigm that utilises fiber-optic ultrasound sources and detectors to perform pulse-echo imaging. Using rapid-prototyping techniques, flexible fiber-optic free-hand probes, capable of video-rate imaging can be constructed entirely from glass and plastic. As such, these devices are expected to be inherently compatible with electromagnetic imaging modalities such as magnetic resonance imaging and computed tomography imaging. However, to date, this multimodal capability has not been demonstrated. In this work, a new free-hand optical ultrasound (OpUS) imaging system is introduced, its real-time imaging capability demonstrated on a range of phantoms, and the first concurrent use of OpUS alongside cone-beam CT (CBCT) imaging is presented.

*Index Terms*—Optical Ultrasound, Multimodal Imaging, Computed Tomography, X-ray immunity

## I. INTRODUCTION

Computed tomography (CT) imaging is a widely used imaging technique that offers excellent spatio-temporal resolution, and the capacity for video-rate and 3D imaging. However, CT imaging is hampered by poor soft-tissue contrast, an area in which ultrasound imaging excels. A range of fusion-imaging techniques have been developed that exploit the complementary contrasts that these modalities provide to improve prostate imaging [1], image abdominal aortic aneurysms [2] and monitor therapeutic applications [3]. These techniques all rely on separate ultrasound and CT scans, which are then digitally combined. Real-time ultrasound imaging inside CT systems has been suggested as a method to improve fusion imaging, and may also be used to gate CT imaging based on breathing cycle or heartbeat tracking. Conventional ultrasound imaging probes utilise piezoelectric elements that have been found to attenuate X-rays and induce artefacts in CT images [4], and may also concentrate the X-rays at the probe-skin interface inducing a surface radiation bolus [5]. In order to exploit the possibilities of concurrent CT-ultrasound imaging, radiolucent devices are required. Whilst partially radiolucent piezoelectric ultrasound probes have been fabricated that limit these artefacts and effects [5], further reductions are required.

Optical ultrasound (OpUS) is an ultrasound imaging modality in which ultrasound is both transmitted and detected by optical means [6]. Several studies have suggested that OpUS probes would be inherently electromagnetic (EM)-compatible [7], making OpUS devices a prime candidate for multimodal

imaging combining ultrasound with CT. In an OpUS system, ultrasound is generated via the photoacoustic effect in a coating or membrane [8], [9], which then transmits ultrasound into the imaging volume, and ultrasound is detected through optical means [10]–[12]. Several configurations of OpUS systems have been developed: large bench-top systems [13], small fiber-optic probes [14] and freehand OpUS probes [6].

Freehand OpUS devices are an emerging OpUS imaging paradigm, in which an array of fiber-optic OpUS and a single fiber-optic detector are mounted together to form an imaging probe with a similar form factor to a conventional piezoelectic ultrasound probe [6]. The fiber-optic OpUS sources are illuminated in sequence to form an imaging aperture without requiring mechanical translation of the imaging probe. These probes have demonstrated real-time video-rate ultrasound imaging on small imaging fields, and are compact and flexible. The probe-heads for these devices are constructed entirely from glass and plastic, meaning that they are inherently compatible with EM-imaging modalities [6].

In this work we present, to the authors knowledge, the first demonstration of a free-hand OpUS probe running concurrently with CT imaging. A free-hand OpUS probe and mobile OpUS imaging platform were designed and fabricated specifically for use alongside other imaging modalities. The imaging capabilities for this probe were demonstrated on the bench top using a range of imaging phantoms and the system was capable of effective real-time video-rate imaging. The OpUS probe and system were then used to perform OpUS imaging in the bore of a running cone-beam CT (CBCT) imaging system. Comparative imaging of the OpUS imaging probe and a conventional probe were used to demonstrate the improved EM-compatibility, and concurrent CBCT and OpUS imaging was performed on static and dynamic imaging phantoms.

## II. METHODS

### A. Freehand OpUS Imaging Probe

A freehand OpUS probe was fabricated such that it would be capable of imaging at a significant distance from any metallic components. As such, a custom, 11 meter long bundle containing 64 optic fibers (diameter:105 μm; Thorlabs; FG105LCA) was fabricated. The proximal end of the bundle was formed into two rows of stripped and flat-cleaved fibers bonded to an acrylic substrate at 400 μm pitch to allow for light to be coupled into the fibers. The distal end of the bundle comprised a single row of fibers at 400 μm pitch, stripped and

set between two pieces of acrylic. The full distal end was then laser-cut and manually polished to form a flat array of fibers. Eccentric sources have previosuly been demonstrated to improve ultrasound pressure confinement to the intended imaging plane, thus improving imaging depth [15]. To generate eccentric sources by shaping the light output from the bundle, an array of 64 eccentric (0.2 mm wide by 1 mm tall by 10 mm long) optical waveguides were fabricated [15]. For ultrasound detection, a fiber-optic Fabry-Pérot detector was positioned centrally in the imaging plane, by printing one waveguide in the array at 0.8 mm tall, resulting in the detector face resting approximately 300 μm above the intended imaging plane.

To generate OpUS an elemental carbon-loaded poly-dimethylsiloxane (PDMS) membrane [16] was bonded to the front face of the waveguide array by uncured, carbon-loaded PDMS. The distal end of the fiber bundle was then butt-coupled to the waveguide array and held in place by a custom printed coupler. The entire distal end of the probe was housed in a printed polylactic acid (PLA) clamshell with dimensions 60 mm (width) by 21 mm (height) by 91 mm (long), and two strain-relief sections printed in elastic resin (FLELCL01 Elastic Resin 50a V1, Formlabs).

### B. Mobile OpUS Imaging Platform

To facilitate OpUS imaging outside of the laboratory a self contained, mobile OpUS imaging platform was constructed inside a mobile 19-inch server rack. System control and data acquisition was achieved with a rack-mounted blade-PC (PC: Precision 3930 Rack, Dell Corporation, Tx, USA; CPU: Intel Core i7-8700K, RAM: 128 GB) with an internal data acqui-sition card (sampling frequency: 250 MHz; bit-depth: 16 bits; M4i.4420-x8, Spectrum, Germany) and graphical processing unit (GPU; Quadro P6000, NVIDIA Corporation, CA, USA). This system was capable of running custom GPU-enabled ultrasound beamformers in real time [17].

The fiber-optic Fabry-Pérot detector mounted inside the freehand OpUS probe was interrogated by a continuous-wave light source (TUNICS T100S-HP, EXFO, Canada) that was continuously tuned to the wavelength corresponding to the greatest pressure sensitivity [11] and delivered to the detec-tor through a circulator (6015-3-APC, Thorlabs, Germany). Reflected light was detected using a custom photodetector.

To generate OpUS from the freehand probe, pulsed excita-tion light (wavelength:1064 nm; pulse duration: 1.5 ns; pulse repetition rate: 2.5 kHz; DSS1064-Q3, Crylas, Germany) was sequentially coupled into the proximal ends of the fibers by a set of galvanometers (GVS002, Thorlabs, Germany) and a scan lens (focal length, 110 mm; field of view: 28.9 mm × 28.9 mm; LSM05-BB, Thorlabs, Germany ) to synthesise an image aperture at the distal end of the probe.

### C. Probe Characterisation

The freehand OpUS probe was characterised by a field scan with a calibrated needle hydrophone (Calibrated bandwidth: 1-30 MHz, diameter 200 μm, Precision Acoustics), at 20%

laser power (pulse energy: 14.2 μJ) to preserve optical com-ponents over the extended duration (*ca.* 54 h) of the scan. Subsequently, the on-axis performance of each element was characterized with the laser at maximum power (pulse energy: 71 μJ) to match the ultrasound generated in an imaging sce-nario. The imaging performance of the probe was determined by imaging a single tungsten wire (diameter: 27 μm; acting as a point target) located centrally in the imaging plane.

### D. CBCT Imaging

To facilitate CBCT imaging and avoid radiation dose to the operator, an acrylic frame was fabricated to hold the freehand probe in place during imaging. The frame and a waterbath were then placed centrally in the bore of the CBCT system (O-arm scanner, Medtronic, Dublin, Ireland). The freehand OpUS probe was then fixed on the frame and concurrent CBCT-OpUS imaging was performed on a range of wire target phantoms, a dynamically inflated balloon phantom and a tissue-mimicking vessel phantom. OpUS video imaging data was collected during the acquisition of 3D CBCT scans, and CBCT scans were repeated for each phantom with and without the OpUS device running. Equivalent CBCT scans were also collected with an inactive, conventional piezoelectric ultra-sound imaging probe (C1-5-D curved linear array transducer, GE HealthCare Technologies Inc., Il, USA).

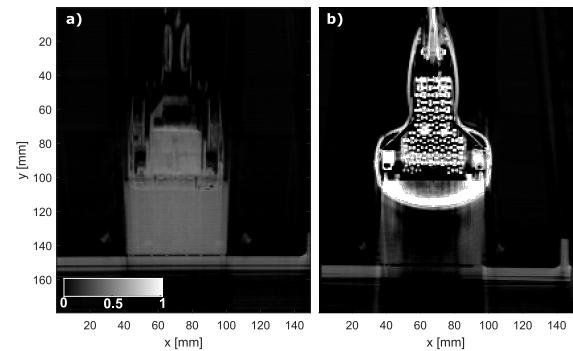## III. RESULTS

### A. Comparative CT imaging



Fig. 1. **Comparative cone-beam CT imaging of freehand OpUS and conventional piezoelectric ultrasound probe. a)** CBCT image of freehand OpUS probe held in empty water bath. **b)** CBCT image of 2D piezoelectric ultrasound probe

Comparative CBCT imaging of both the freehand OpUS probe described here and a conventional piezoelectric imaging probe, each partially submerged in a waterbath, demonstrate the significant artefacts induced by the metallic elements in the piezoelectric device (figure 1). There is significant shadowing induced in the area below the piezoelectric probe, this is so significant that over 50% of the voxels in the area below the piezoelectric probe recorded zero signal. In addition to this there is significant signal confined to the probe face, in line with the surface bolus described by Schlosser and Hristov [5].
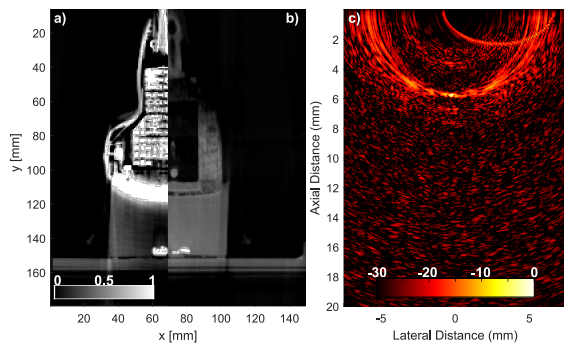
Fig. 2. **Comparative CBCT images of tungsten wire phantom and OpUS image of wire phantom a)** CBCT image of piezoelectric probe over tungsten wire phantom in water bath. **b)** CBCT image of OpUS probe held over tungsten wire phantom in water bath. **C)** OpUS image captured during active CBCT acquisition of tungsten wire phantom in water bath, used for resolution calculation.

These effects are minimised by the OpUS probe, with only a slight shadowing induced by the edges of the probe clamshell, and no artefacts induced by the active probe elements. To quantify the effect of the piezoelectric probe an average pixel value was calculated from the CBCT signal in the waterbath below the imaging probe, aligned to the approximate location of the ultrasound iamging plane for each probe. For water with no probe present the average value was $0.37 \pm 0.06$ (mean $\pm$ standard deviation), for water with the OpUS probe present this value was $0.39 \pm 0.01$ and for water with the piezoelectric probe present this value was $0.06 \pm 0.08$. With the piezoelectric probe 52% of the pixels in the target area generated no signal.

### B. OpUS Probe Performance

Field scans revealed that three of the fibers in the probe had become damaged, resulting in 61 active sources in the array. At a distance of 1.6 mm the remaining sources exhibited a peak pressure of $0.14 \pm 0.08$ MPa (mean $\pm$ standard deviation), a high center frequency of $10.8 \pm 1.2$ MHz and $-6$ dB bandwidth of $18.6 \pm 2.3$. The angular spectrum approach (ASA) [18] was used to back-propagate all sources to the surface of the probe, and demonstrated that the sources were eccentric and matched the size and patterning of the underlying waveguide structure. This propagation also demonstrated that the generated OpUS fields were highly directional in the elevational axis, effectively confining ultrasound pressure to the imaging plane.

OpUS images of a point-like structure yielded spatial resolutions of 171 μm (axial) by 259 μm (lateral) with a conventional DAS beamformer. However, this imaging is limited by the residual grating lobe artefacts consistent with imaging with low channel counts and large inter-element pitch, as was previously observed with freehand OpUS devices [6]; as a result, the imaging was limited by a signal-to-clutter (SCR) of 23 dB. The imaging system could image at up to 24 Hz, with real-time DAS image reconstruction, visualisation and data saving. However, to improve image quality whilst retaining

video-rate imaging threefold averaging was used for all future imaging tests, achieving a framerate of 10 Hz.

### C. Concurrent OpUS-CT Imaging

Concurrent CBCT-OpUS imaging was conducted with a range of phantoms. To assess CBCT impact on OpUS imaging OpUS video imaging of an empty water bath. The average pixel value in the waterbath was calculated for both OpUS and CBCT for concurrent and separate imaging. In video OpUS imaging there was only a 0.09% difference in mean pixel value and identical standard deviation for both independent and CBCT-concurrent imaging. Likewise, there was only a 0.18% difference in average pixel values for CBCT imaging with and without concurrent OpUS imaging. Using the probe face and central location of the fibre optic receiver as reference points, manual overlays of OpUS and CT were generated, and demonstrated accurate mapping of target positions in the imaging plane.

To demonstrate the dynamic nature of freehand OpUS imaging with simultaneous CBCT imaging, a latex balloon was repeatedly inflated and deflated, effectively moving a highly echogenic scattering surface (the water-balloon-air interface) vertically in the OpUS imaging field. Under CBCT imaging this had the effect of a repeatedly expanding and contracting air bubble moving during the 3D acquisition process, inducing motion artefacts in the CBCT scan. OpUS imaging of this process accurately visualised the moving interface, without any additional artefacts from CBCT (figure 3).

### IV. DISCUSSION AND CONCLUSION

In this work a novel freehand OpUS imaging probe and accompanying mobile imaging platform are presented. This probe comprised 61 eccentric OpUS sources and a single fiber-optic Fabry-Pérot detector, fabricated into an 11 m long custom fiber-optic bundle and was capable of real-time imaging at up to 24 Hz. This probe was then used to image a range of imaging targets and dynamic motion phantoms concurrently with CBCT. Neither modality demonstrated any significant impact from the presence and action of the other system, and when compared to a conventional piezoelectric ultrasound probe, the freehand OpUS probe demonstrated negligible impact on the quality of the CBCT images.

The freehand OpUS imaging probe presented here demonstrates a step forwards in the design of this type of device, specifically built to target multimodal applications. This probe design encapsulates several significant improvements from earlier designs including: an improved absorbing membrane recipe for more even ultrasound generation, an array of 64 3D printed waveguides to generate eccentric sources, a Fabry-Pérot detector located centrally in the imaging plane and a functionally protected probe design. This design is the first freehand OpUS device that has the capacity for imaging experiments outside of the laboratory, and is a significant step closer to a clinically relevant imaging system. However,the imaging quality demonstrated by this probe was significantly hampered by the low channel count and element size. With
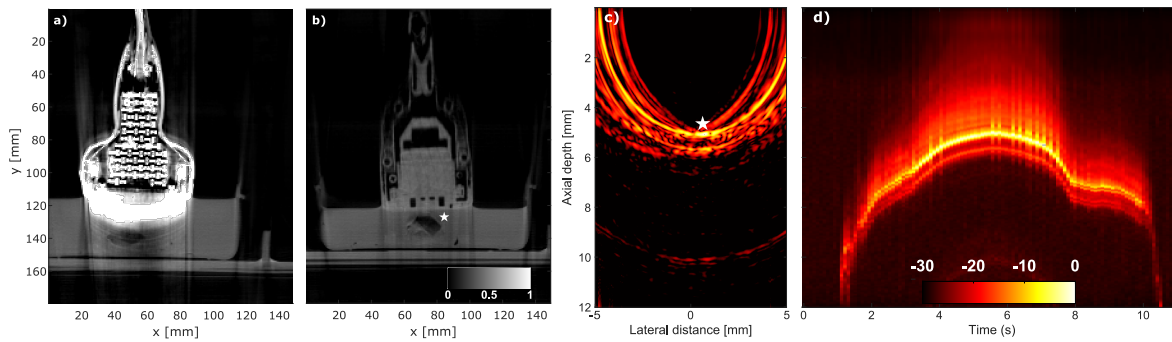
Fig. 3. **Concurrent CBCT-OpUS imaging of dynamic balloon inflation process. a)** CBCT image of piezoelectric ultrasound probe taken during repeated inflation of balloon phantom **b)** CBCT image of freehand OpUS probe taken during OpUS imaging of repeated inflation of balloon phantom, top surface of balloon marked with ⋆ **c)** Freehand OpUS image of inflated balloon phantom, top surface of balloon marked with ⋆ **d)** M-mode OpUS image of a single balloon inflation during simultaneous 3D CBCT acquisition, comprising concatenated laterally averaged signals, captured with single averaging at 24 Hz.

only 61 sources, significant side-lobe artefacts were induced that impact the signal to clutter ratio, and the 400 µm element pitch induces significant grating lobes. The imaging quality of the probe could be improved by increasing the number of sources and reducing the inter-element pitch. With the methods presented in this work, this would require an alternative method of generating eccentric sources [15].

This work presents, to the authors knowledge, the first demonstration of real-time concurrent CT and OpUS imaging, and as such confirms that OpUS devices are inherently compatible with X-ray imaging modalities, with neither OpUS or CBCT image quality being significantly impacted by the presence of the complimentary modality. Imaging studies of phantoms that were not visible in CBCT but were clearly seen under OpUS also indicates the potential for improved multimodal imaging with OpUS during CT-guided procedures. The level of EM immunity demonstrated here further suggests the presented imaging probe is compatible with other EM-based imaging modalities such as magnetic resonance imaging (MRI). Compatibility between CT and OpUS also indicates the possibility that OpUS devices would be suitable for use alongside ionising-radiation based treatment modalities such as external-beam radiation therapy (EBRT). Freehand OpUS imaging probes thus show significant promise for clinical application, offering high frame rates, versatile operation, and negligible image artefacts and mutual interference when applied concurrently with CBCT imaging.

## REFERENCES

[1] D. Bowes, J. M. Crook, C. Araujo *et al.*, "Ultrasound-ct fusion compared with mr-ct fusion for postimplant dosimetry in permanent prostate brachytherapy," *Brachytherapy*, vol. 12, pp. 38–43, 2013. [Online]. Available: http://dx.doi.org/10.1016/j.brachy.2012.03.007

[2] G. Zur, M. Andraous, E. Bercovich *et al.*, "Ct-ultrasound fusion for abdominal aortic aneurysm measurement," *American Journal of Roentgenology*, vol. 214, pp. 472–476, 2020.

[3] W. Wein, B. Röer, and N. Navab, "Automatic registration and fusion of ultrasound with ct for radiotherapy," *Lecture Notes in Computer Science (including subseries Lecture Notes in Artificial Intelligence and Lecture Notes in Bioinformatics)*, vol. 3750 LNCS, pp. 303–311, 2005.

[4] M. Bazalova-Carter, J. Schlosser, J. Chen *et al.*, "Monte carlo modeling of ultrasound probes for image guided radiotherapy," *Medical Physics*, vol. 42, pp. 5745–5756, 2015.

[5] J. Schlosser and D. Hristov, "Radiolucent 4d ultrasound imaging: System design and application to radiotherapy guidance," *IEEE Transactions on Medical Imaging*, vol. 35, pp. 2292–2300, 2016.

[6] E. J. Alles, E. C. Mackle, S. Noimark *et al.*, "Freehand and video-rate all-optical ultrasound imaging," *Ultrasonics*, vol. 116, p. 106514, 2021. [Online]. Available: https://doi.org/10.1016/j.ultras.2021.106514

[7] E. J. Alles, N. F. Sheung, S. Noimark *et al.*, "A reconfigurable all-optical ultrasound transducer array for 3d endoscopic imaging," *Scientific Reports*, vol. 7, pp. 1–9, 2017. [Online]. Available: http://dx.doi.org/10.1038/s41598-017-01375-2

[8] P. Beard, "Biomedical photoacoustic imaging," *Interface focus*, vol. 1, pp. 602–631, 2011.

[9] S. Noimark, R. J. Colchester, B. J. Blackburn *et al.*, "Carbon-nanotube – pdms composite coatings on optical fibers for all-optical ultrasound imaging," *Advanced Functional Materials*, vol. 26, pp. 8390–8396, 2016.

[10] J. L. Johnson, M. Merrilees, J. Shragge *et al.*, "All-optical extravascular laser-ultrasound and photoacoustic imaging of calcified atherosclerotic plaque in excised carotid artery," *Photoacoustics*, vol. 9, pp. 62–72, 2018. [Online]. Available: https://doi.org/10.1016/j.pacs.2018.01.002

[11] J. A. Guggenheim, J. Li, T. J. Allen *et al.*, "Ultrasensitive plano-concave optical microresonators for ultrasound sensing," *Nature Photonics*, vol. 11, pp. 714–719, 2017.

[12] W. J. Westerveld, M. Mahmud-Ul-Hasan, R. Shnaiderman *et al.*, "Sensitive, small, broadband and scalable optomechanical ultrasound sensor in silicon photonics," *Nature Photonics*, vol. 15, pp. 341–345, 2021. [Online]. Available: http://dx.doi.org/10.1038/s41566-021-00776-0

[13] E. J. Alles, S. Noimark, E. Maneas *et al.*, "Video-rate all-optical ultrasound imaging," *Biomedical optics express*, vol. 9, pp. 3481–3494, 2018.

[14] E. J. Alles, S. Noimark, E. Zhang *et al.*, "Pencil beam all-optical ultrasound imaging," *Biomedical Optics Express*, vol. 7, p. 3696, 2016.

[15] F. T. Watt, S. Noimark, A. E. Desjardins *et al.*, "Fabrication of an array of eccentric sources for freehand optical ultrasound imaging," in *2022 IEEE International Ultrasonics Symposium (IUS)*. IEEE, 2022, pp. 1–4.

[16] E. J. Alles, "Rapid non-contact optical ultrasound for biomedical imaging," in *2023 IEEE International Ultrasonics Symposium (IUS)*. IEEE, 2023 in press.

[17] F. T. Watt, P. C. Beard, and E. J. Alles, "Developing real-time implementations of non-linear beamformers for enhanced optical ultrasound imaging," in *2022 IEEE International Ultrasonics Symposium (IUS)*, 2022.

[18] X. Zeng and R. J. McGough, "Optimal simulations of ultrasonic fields produced by large thermal therapy arrays using the angular spectrum approach," *The Journal of the Acoustical Society of America*, vol. 125, p. 2967, 2009.